Supplementary Information (SI) for Nanoscale.

This journal is © The Royal Society of Chemistry 2025

Supplementary Information

Crosslinking confined charge-transfer complex for the construction of photo-responsive hydrogels

Menglin Wu,[a] Baochuan Zhang,[b] Pengcheng Wang,[b] Tongyu He,[b] Xin Jiang,[b] Lulu Qian,[b] Mingyue Cui,*[a,b] Bin Song,*[b] and Yao He*[a,b]

[a] Macao Translational Medicine Center, Macau University of Science and Technology, Taipa 999078, Macau SAR, China.

[b] Suzhou Key Laboratory of Nanotechnology and Biomedicine, Institute of Functional Nano & Soft Materials & Collaborative Innovation Centre of Suzhou Nano Science and Technology (NANO-CIC), Soochow University, Suzhou 215123, China.

*Corresponding author.

E-mail: mingyuecui@suda.edu.cn; bsong@suda.edu.cn; yaohe@suda.edu.cn

Experimental Procedures

Materials. (3-Aminopropyl) trimethoxysilane (APTMS) (97%) and Polyvinyl alcohol (Mw = 89,000-98,000, PVA) are purchased from Sigma-Aldrich. 1,8-Naphthalimide (NA) is purchased from Jiangsu Argon Krypton Xenon Technology Co., Ltd. Boric acid (Mw = 61.83, BA) and Polyvinylpyrrolidone (PVP) are bought from Cin.diff Biotechnology Co.,Ltd (Shanghai, China). Milli-Q water is used as the solvent for preparing samples. All the chemicals are used without further purification.

Preparation of SiNPs. The SiNPs precursor solution is prepared by mixing 5 mL of APTMS and 20 mL of ultrapure water. The mixture is stirred adequately at room temperature for 3 hours. After that, the fully dissolved precursor solution is placed into an autoclave. Then, it is put in an oven with 190 °C for 3 h and cooled to 30 °C naturally.

Preparation of NA modified SiNPs. The NA modified SiNPs are prepared by mixing 0.1 g of NA and 2 mL of SiNPs. The mixture is then irradiated under a high-power ultraviolet lamp for 5, 10, 20, and 30 minutes. After irradiation, centrifuge the solution at 12,000 rpm for 3 minutes, and collect the supernatant for later use.

Preparation of light responsive NASiNPs-based hydrogel composites. The hydrogel composite materials based on NASiNPs are fabricated by mixing 2.1 g of PVA with 0.3 g of NA, along with 0.1 g of PVP as a stabilizing agent. Subsequently, 25 mL of SiNPs solution is incorporated and stirred in a water bath maintained at a constant temperature of 90°C for a duration of 2 hours, until the solution clarifies. Next, 0.2 g of BA is dissolved in 10 mL of ultrapure water and preheated in a water bath at 60°C. Finally, 8 mL of the boric acid aqueous solution is added to the gel precursor and thoroughly mixed. Upon cooling to room temperature, a uniform and stable hydrogel system is developed.

Rheological performance testing. An appropriate amount of gel is placed on the temperature-controlled software of a rotational rheometer, with the environmental temperature set to 90°C, a 40 mm steel plate is used as the fixture, with a gap of 1000 μm set under heating conditions, followed by testing at 25°C.

Characterization of self-healing properties. The hydrogel is cut into two halves at room temperature, and the hydrogel is repaired for 20 s without external stimulation. The repair is observed with naked eyes; Simultaneously irradiate with ultraviolet light source and observe the luminescent properties during the repair process. The stereomicroscope is used to observe the crack state of the gel after repairing for 0s, 20s, 40s and 60s. The tensile stress of the original gel and the repair at four time points of 1 min, 10 min, 30 min and 60 min are measured respectively by using a microcomputer controlled electronic universal testing machine, and the self-repairing efficiency is calculated. The formula is: self-healing efficiency (η)= (self-healing time train (%)/(original train (%) × 100%.

Computational details. All geometry optimizations were performed using the Gaussian 16 software package at the B3LYP-D3BJ/6-31G(d,p) level of theory. Ground-state geometry optimizations are carried out using Density Functional Theory (DFT), while excited-state geometry optimizations are performed using time-dependent DFT (TD-DFT). Molecular orbital analysis and molecular electrostatic potential (ESP) mapping are computed at the same B3LYP level of theory. Visualizations are performed using the Multiwfn and VMD programs[1-3]. The reduced density gradient (RDG) analysis for the photo-induced charge-transfer complex NASiNPs is also conducted using Multiwfn, with plotting done in VMD. The SiNPs donor model was constructed based on 3-aminopropylsilanetriol (H_2N–$(CH_2)_3$–$Si(OH)_3$), representing the hydrolysis product of APTMS. The selected charge-transfer complex is pre-calculated at the B3LYP-D3BJ/6-31G(d) level in Gaussian 16 to obtain electron density. For binding energy calculations of the charge-transfer complex NASiNPs in the ground state, the energies of NASiNPs, NA, and SiNPs are taken as the minimal energies obtained after geometry optimization. The binding energy is calculated as: E(NASiNPs)−E(NA)−E(SiNPs). For the excited state, the binding energy is calculated as: E([NASiNPs]∗)−E(NA∗)−E(SiNPs). Where E([NASiNPs]*), E(NA*) and E(SiNPs) refer to the minimal energies obtained after geometry optimization of the excited-state species. Additionally, the Gibbs free energy is obtained by performing geometry optimization at the B3LYP-D3BJ/6-31G(d,p) level of theory.

Characterization. Transmission electron microscopy (TEM) and scanning TEM (STEM) images are acquired using a Talos 200X electron microscope operated at 200 kV. Energy-dispersive X-ray (EDX) spectroscopy is employed to determine the elemental composition of the prepared samples. Fourier transform infrared (FTIR) spectra are recorded using a Bruker FTIR spectrometer with a resolution of 4 cm^{-1}. X-ray photoelectron spectroscopy (XPS) analysis is performed using a Kratos AXIS Ultra DLD system. Scanning electron microscopy (SEM) is conducted on a ZEISS Gemini 500, with hydrogels freeze-dried and gold-coated via sputtering. Electron spin resonance (ESR) measurements are carried out on a JES-X320 spectrometer at 123 K. Photoluminescence (PL) spectra are obtained using a Hitachi F-4700 fluorescence spectrophotometer. Time-resolved fluorescence lifetime measurements are performed with an Edinburgh FLS 980 fluorescence spectrometer, using a microsecond flash lamp as the excitation source in single-photon counting multi-channel scaling mode. Rheological properties are analyzed with a Thermo HAAKE MARS 60 rotary rheometer, using a 40 mm diameter serrated antiskid parallel plate with a 3° cone angle. Strain sweep and frequency sweep experiments are conducted over ranges of 0.1 to 1000% and 0.1 to 100 rad/s, respectively.

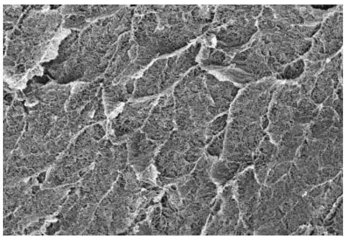

Figure S1. SEM image of pure PVA.

The freeze-dried PVA is imaged using scanning electron microscopy (SEM) at various magnifications. The SEM images reveal a smooth surface with distinct crack-like structures, characteristic of the freeze-drying process.

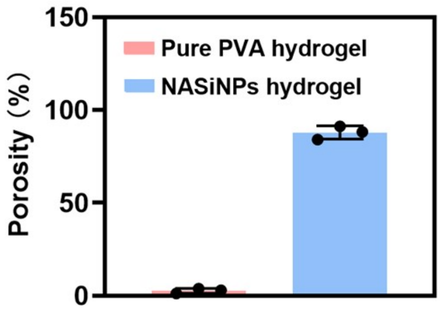

Figure S2. The porosity of NASiNP hydrogel and pure PVA hydrogel.

As illustrated in Figure S2, the porosity of NASiNP hydrogel (~87.8%) is significantly higher than that of pure PVA hydrogel (~2.6%). This enhanced porosity not only facilitates water diffusion and polymer chain mobility, but also contributes to the improved mechanical elasticity and rapid self-healing behavior observed in the NASiNP hydrogel system.

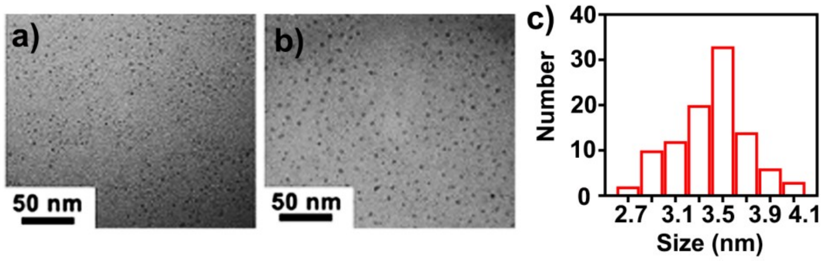

Figure S3. a) transmission electron microscopy (TEM) images of SiNPs and b) NASiNPs. c) The quantitative size distribution of the as-prepared NASiNPs.

To determine the structure of SiNPs and NASiNPs, their morphologies are characterized by TEM. As shown in Figure S3a and b, both the as-prepared pure SiNPs and NASiNPs exhibit a uniform size distribution. The analysis of over 100 NASiNPs reveals a narrow size distribution with an average diameter of 3.5 ± 0.4 nm (Figure S3c).

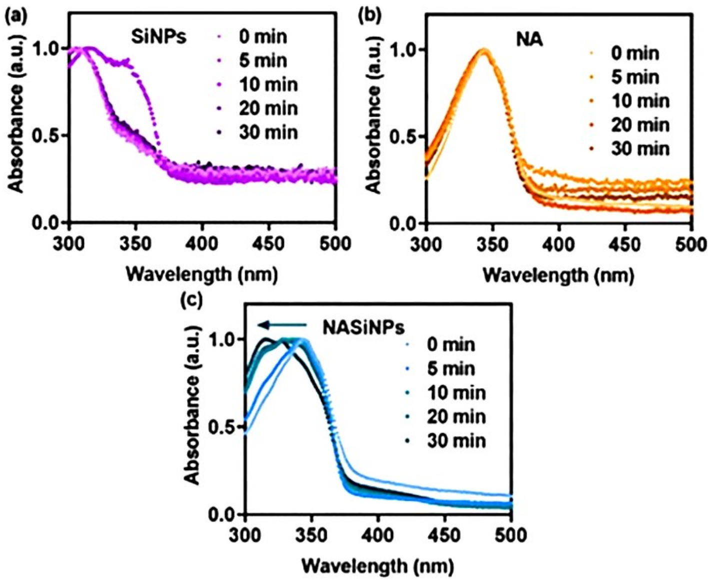

Figure S4. Normalized absorbance spectra of the (a)SiNPs, (b)NA and (c)NASiNPs mixture before and after UV irradiation.

The UV absorption spectra of SiNPs, NA, and NASiNPs are measured separately. Compared to NA and SiNPs, the UV absorption spectrum of NASiNPs exhibits a blue shift as the UV irradiation time increases.

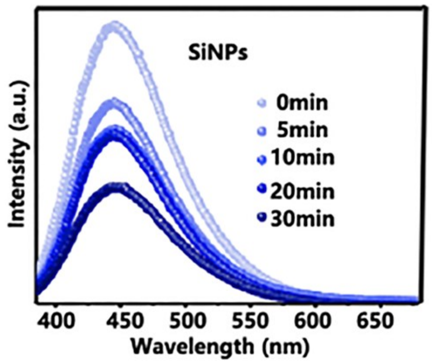

Figure S5. Fluorescence spectra of SiNPs during 30 min of UV irradiation.

As the UV irradiation time increases from 0 to 30 minutes, the maximum emission wavelength of SiNPs remains unchanged, while the intensity gradually decreases.

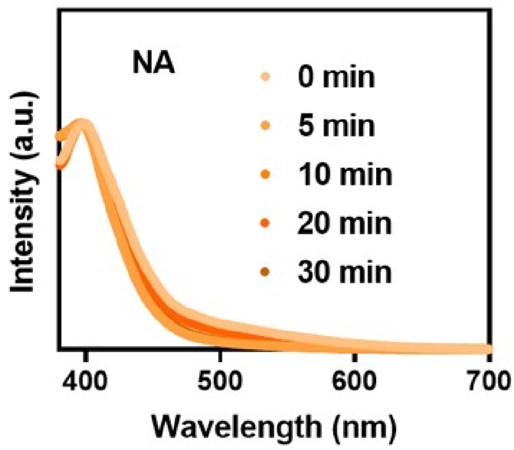

Figure S6. Normalized fluorescence spectra of the NA during 30 min UV irradiation.

The fluorescence spectra of NA before and after UV irradiation show a stable blue fluorescence peak at 400 nm.

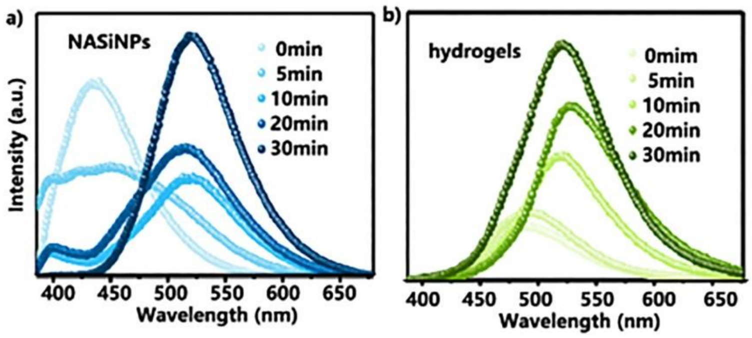

Figure S7. Fluorescence spectra of NASiNPs (a), and hydrogels (b) during 30 min of UV irradiation.

As the UV irradiation time increases from 0 to 30 minutes, the maximum emission wavelength of NASiNPs and hydrogels demonstrates dramatically redshift from 440 nm to 525 nm.

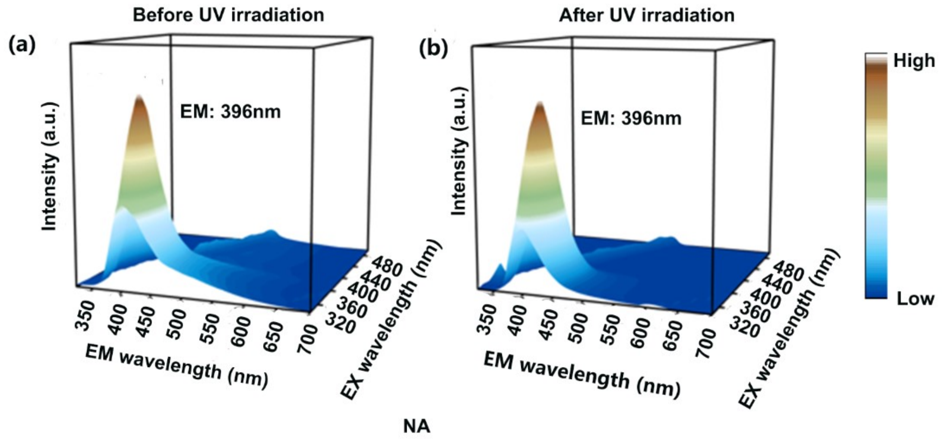

Figure S8. Changes in 3D fluorescence spectra of NA. 3D excitation-emission correlated fluorescence spectra of NA (a) before (left) and after (right) UV irradiation.

The 3D fluorescence peak characteristics of NA remain essentially unchanged before and after UV treatment.

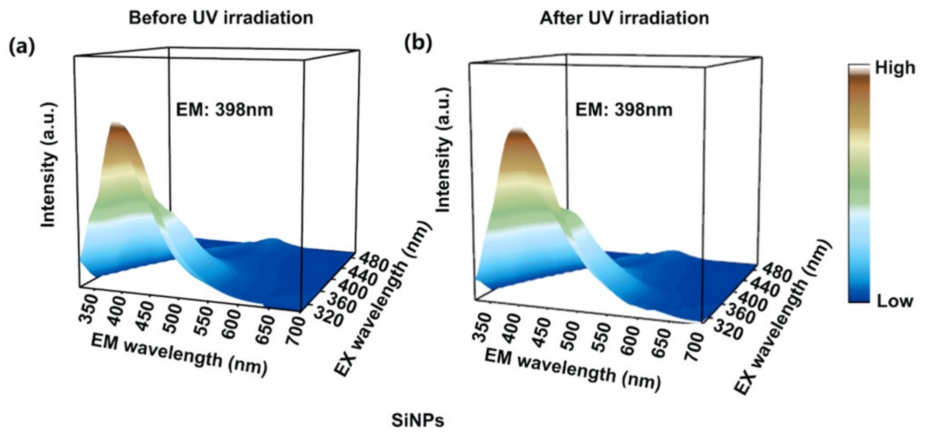

Figure S9. Changes in 3D Fluorescence Spectra of SiNPs. 3D excitation-emission correlated fluorescence spectra of SiNPs (a) before (left) and (b) after (right) UV irradiation.

The 3D fluorescence peak characteristics of SiNPs remain essentially unchanged before and after UV treatment.

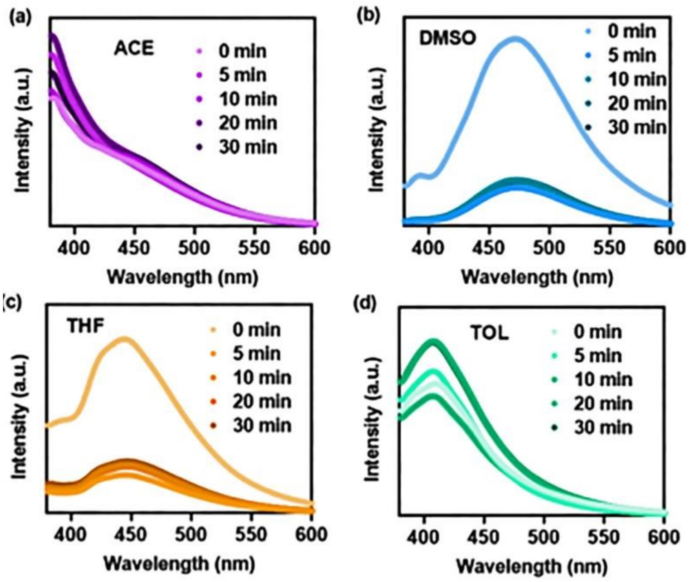

Figure S10. Emission spectra in different solvents. Fluorescence emission spectra (λ_{ex} = 360 nm) of NASiNPs mixture before and after UV irradiation in (a) acetone (ACE), (b) dimethyl sulfoxide (DMSO), (c) tetrahydrofuran (THF) and (d) toluene (TOL).

To evaluate the effect of solvents on the fluorescence emission spectra of NASiNPs, the resultant samples are dissolved in various solvents. Among the four groups, the peak position of the emission spectrum of NASiNPs remains stable before and after UV irradiation.

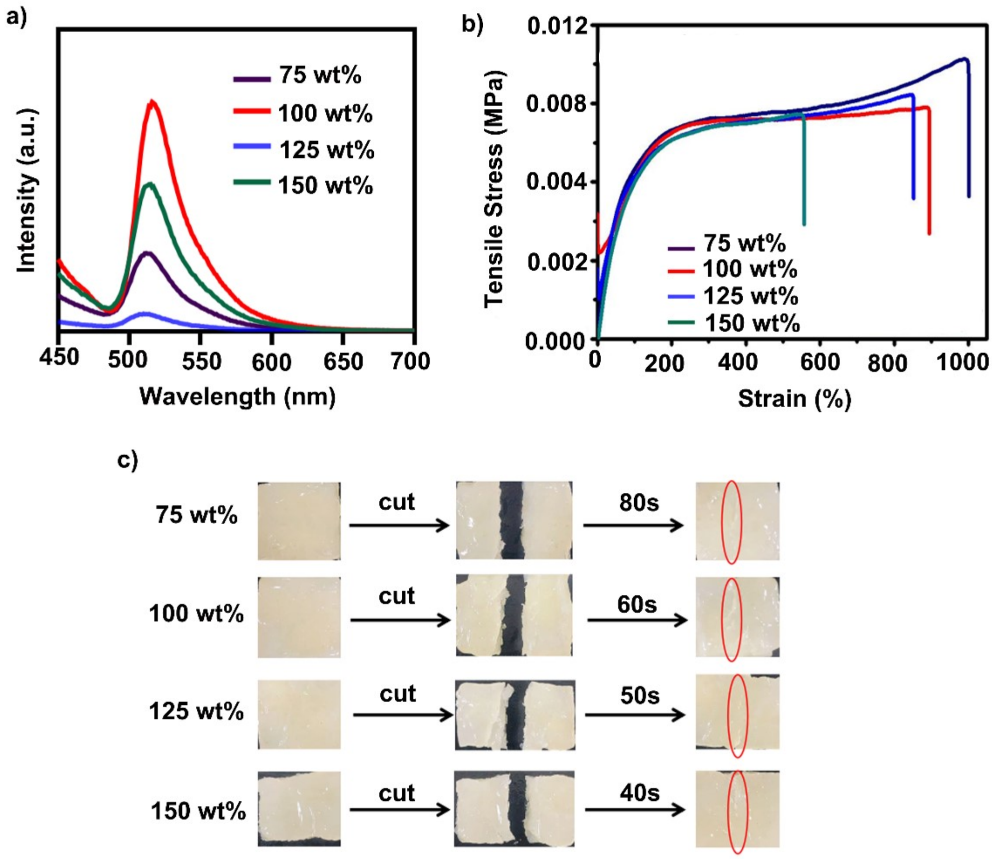

Figure S11. The effect of NASiNP concentration on the a) fluorescence characteristics, b) mechanical properties and c) self-healing efficiency of the hydrogel.

As shown in Figures S11, increasing NASiNP content significantly modulates the hydrogel’s fluorescence intensity and mechanical strength. Moreover, higher NASiNP loading enhances self-healing efficiency by accelerating the recovery process. Notably, the hydrogel with 100 wt% NASiNPs exhibits the strongest emission, high elasticity, and rapid healing (60 s), representing the optimal formulation among all tested compositions.

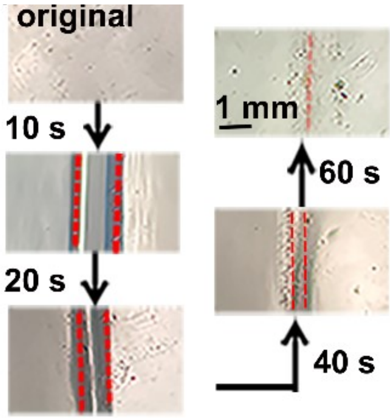

Figure S12. Optical images of the hydrogels during the self-healing process.

Figure S12 shows the microscopic images of the fracture healing process in the hydrogels. The cracks nearly disappear within 60 seconds, demonstrating the hydrogels excellent self-healing properties.

Table S1 PLQY of SiNPs and NASiNPs during 30min UV irradiation.

UV irradiation time (min)	SiNPs	NASiNPs
0	12.7%	3.3%
5	11.4%	3.1%
10	10.5%	3.0%
20	9.0%	3.6%
30	8.4%	3.9%

Table S2 Summary of photo-responsive performance and mechanical properties of representative hydrogel systems.

Material	Response time	Emission shift (nm)	Elastic strain (%)	Self-healing efficiency y / Time	Reference
poly(γ-glutamic) acid hydrogels	---	---	200%	97.5% / 3 h	Nanoscale, 2018, 10.
BSiNP/Polyvinyl alcohol hydrogels	---	85	281%	~91.5% / 1 h	*Anal. Chem.* 2022, 94.
Ion/Poly(acrylic acid hydrogels	~3 min	---	190%	---	Adv. Mater. 2019, 31.
Polyvinyl alcohol/borax hydrogels	~30 min	44	---	---	Adv. Funct. Mater. 2021, 31.
Poly(acrylic acid)/TPYA Hydrogel	~30 min	---	300%	~100% / 24 h	ACS Appl. Mater. Interfaces 2019, 11,
NASiNPs/ Polyvinyl alcohol hydrogels	~20 min	~85	475%	~92% / 60 s	*This work*

In summary, compared to previously reported photo-responsive hydrogels, this work presents a multifunctional nanoconfined charge-transfer strategy that simultaneously achieves rapid optical response (~20 min), significant emission red-shift (~85 nm), high elasticity (475%), and efficient self-healing (~92% within 60 s). Such integrated performance surpasses existing systems and highlights the potential of NASiNP-based hydrogels for next-generation intelligent materials in sensing, encryption, and bio-adaptive applications.

References

[1] T. Lu. J. *Chem. Phys*. **2024**, *161*, 082503.

[2] T. Lu, F. J. Chen. *Comput. Chem*. **2012**, *33*, 580-592.

[3] W. Humphrey, A. Dalke, K. J. Schulten. *Molec. Graphics* **1996**, *14*, 33-38.